Polypropylene/Clay Nanocomposites Prepared by *In Situ* Grafting-Melt Intercalation with a Novel Cointercalating Monomer

Pingan Song,[1] Lifang Tong,[1] Zhengping Fang[1,2]

[1]*Institute of Polymer Composites, Zhejiang University, Key Laboratory of Macromolecular Synthesis and Functionalization, Ministry of Education, Hangzhou 310027, China*
[2]*Department of Biochemical and Chemical Engineering, Ningbo Institute of Technology, Zhejiang University, Ningbo 315100, People's Republic of China*

Received 26 September 2007; accepted 6 May 2008
DOI 10.1002/app.28689
Published online 9 July 2008 in Wiley InterScience (www.interscience.wiley.com).

ABSTRACT: Polypropylene (PP)/clay nanocomposites were prepared by melt-compounding PP with organo-montmorillonite (OMT), using maleic anhydride grafted polypropylene (PP-*g*-MA) as the primary compatibilizer and *N*-imidazol-*O*-(bicyclo pentaerythritol phosphate)-*O*-(ethyl methacrylate) phosphate (PEBI) as the cointercalating monomer. X-ray diffraction patterns indicated that the larger interlayer spacing of OMT in PP was obtained due to the cointercalation monomer having a large steric volume and the *d*-spacing further increased with the addition of PP-*g*-MA, as evidenced by transmission electron microscopy. Thermogravimetric analysis revealed that the PEBI-containing PP nanocomposites exhibited better thermal stability than PEBI-free PP composites. Dynamic mechanical analysis demonstrated that the storage modulus was significantly enhanced, and the glass transition temperature (T_g) shifted slightly to low temperature with the incorporation of clay for PP/OMT hybrids. PEBI-containing PP/OMT composites gave a lower T_g value because of the strong internal plasticization effect of PEBI in the system. Cone calorimetry showed that the flame-retardancy properties of PP nanocomposites were highly improved with the incorporation of PEBI. © 2008 Wiley Periodicals, Inc. J Appl Polym Sci 110: 616–623, 2008

Key words: polypropylene; nanostructure; thermal properties; flame retardant

INTRODUCTION

Polymer–clay nanocomposites are a new class of filled polymers in which clay platelets at the nanometer scale are dispersed in the polymer matrix. These nanocomposites exhibit enhanced properties at very low filler loading, usually less than 5 wt %, such as storage modulus, thermal stability and gas barrier properties, and flame retardancy compared with those of neat matrix polymers or conventional micro or macrocomposites.[1–10] Polymer nanocomposites can be synthesized by three primary strategies: melt blending,[5] solution compounding,[11] and *in situ* intercalating polymerization.[12] The first strategy works well with polar polymers such as polysiloxanes, polyesters, and polystyrene,[13] whereas the second strategy is applied to polymers soluble in water,[12] and the third strategy involves a silicate, which can be intercalated by an initiator or catalyst, then an intercalated or exfoliated polymer nanocomposite is formed.[14]

Despite polypropylene (PP) is one of the most widely used polyolefin polymers, the preparation of PP-silicate nanocomposites remains a scientific challenge because of its nonpolarity. Besides, organically modifying inorganic montmorillonite, the formation of PP/montmorillonte nanocomposites usually needs a compatibilizer such as PP-*g*-MA including a certain amount of polar groups, which can be intercalated into silicate layers through hydrogen bonding and be well miscible with PP.[15] Moreover, the dispersion of clay in polymer matrix will be much improved by a high shearing force. Zhang et al.[16] prepared PP/clay nanocomposites, using a swelling agent, and Lin et al.[17] found the basal spacing of clay increased considerably through using epoxypropyl methyacrylate as cointercalating monomer. Dubnikova et al.[18] has recently studied the effects of the maleic anhydride grafted PP (MAPP) kind on both the clay dispersion and miscibility with PP and found that higher MA content (4 wt %) in MAPP increased the

Correspondence to: Z. Fang (zpfang@zju.edu.cn).
Contract grant sponsor: Ningbo City Agency of Science and Technology.

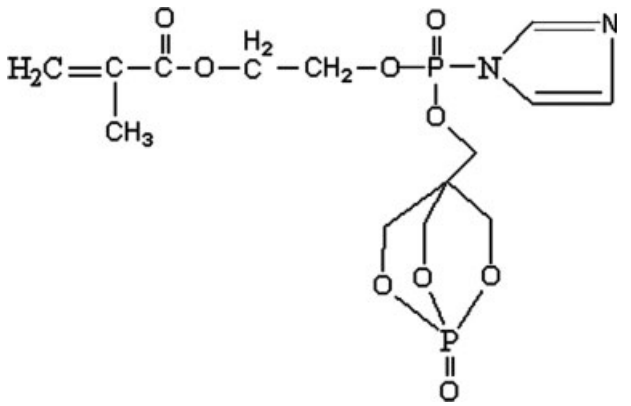

Figure 1 Chemical structure of PEBI.

intercalation ability, however, leading to a poor miscibility with PP matrix.

In this article, we first synthesized a novel flame retardant with a large steric volume, *N*-imidazol-*O*-(bicycli pentaerythritol phosphate)-*O*-(ethyl methacrylate) phosphate (PEBI; shown in Fig. 1) as a cointercalating monomer. Then, we mainly focused on investigating the effect of the large steric volume PEBI on intercalating the organomontmorillonite (OMT) and the effect of PEBI on the flame-retardant properties of PP.

EXPERIMENTAL

Materials

The organically modified clay (OMT) was supplied by Zhejiang Huate Clay Products (Zhejiang, China). It was the product of Na^+-montmorillonite (MMT) ion-changed with bioctadecyl ammonium bromide. PP (S1003, M_n: 38,000) was bought from Shanghai Petrochemicals Factory and PP-*g*-MA (M_n: 21,000, MA: 1 wt %) was obtained from Shanghai Rizhisheng Limited Company. PEBI was self-prepared and hydroethyl methacrylate (HEMA; $CH_2{=}C(CH_3){-}CO{-}OCH_2CH_2OH$, analytic grade) with a smaller steric volume was used as a counterpart to investigate the steric volume effect on increasing the *d*-spacing of clay. All chemicals were used without further purification.

The cointercalating organophilic clay was prepared as follows: a certain amount of dicumyl peroxide (DCP), the initiator of grafting reaction, was first dissolved in 10 mL ethanol. Subsequently, 20 g PEBI or 20 g HEMA were mixed with 60 g OMT for 10 min in a beaker with a stirring speed of 3000 rad/min. The mixtures were dried at 45°C under reduced pressure to eliminate ethanol, and the dry products were designated as PB-OMT and HM-OMT, respectively.

Synthesis of *N*-imidazol-*O*-(bicycli pentaerythritol phosphate)-*O*-(ethyl methacrylate) phosphate

Pentaerythritol (PER; 68 g) and 275 mL dioxane were charged into a four-necked round flask equipped with a magnetic stirrer, reflux condenser, thermometer, addition funnel, dry N_2 inlet, and aqueous NaOH trap. When the reaction temperature reached 95°C, 50% (22.6 mL) of the total $POCl_3$ (0.25 mol) was added. The rest of the $POCl_3$ was dropped at such a rate as to keep the rate of HCl evolution to no more than 2%/min. The reaction finished after about 6–7 h and then was cooled slowly to room temperature and filtered. The white solid was washed once with 50 mL dioxane and twice with 100 mL hexane. The powdery product was dried at 70°C under vacuum to a constant weight (yield: 89%), and the resulting product was named PEPA.

About 36 g (0.2 mol) PEPA, 18 mL (0.2 mol) $POCl_3$, and 250 mL CH_3CN were added to a 500-mL four-necked flask under N_2. When the temperature reached about 80°C, 16.2 mL (0.2 mol) pyridine was dropped slowly into the flask. Afterward, the solution of 100 mL CH_3CN containing 13.6 g (0.2 mol) imidazole and 26 g (0.2 mol) HEMA were dropped into the said flask, and the reaction was continued for another 3 h after the solution was dropped completely. After the reaction was over, CH_3CN was removed under reduced pressure, and the final product, PEBI, could be obtained. Evidence of compound PEBI was presented as following. IR data: 1725 cm^{-1} (C=O), 1640 cm^{-1} (C=C), 1300 cm^{-1} (P=O), 1050 cm^{-1} (P—O—C), 1669 cm^{-1} (C=N), and 1400 cm^{-1}(P—N); ^1H NMR($CDCl_3$, TMS) data: δ = 2.1 ppm (—CH_3, 3H), 3.8–4.0 ppm (—O—CH_2—CH_2—O—, 4H), 4.26 ppm (P—O—CH_2—, 8H), 7.59 ppm (imidazole cycle, 2H), and 9.28 ppm (imidazole cycle, 1H). The synthesis route of compound PEBI was shown in Scheme 1.

Preparation of the PP/clay nanocomposites

A series of nanocomposites were prepared via melt-blending PP with a certain amount of OMT, PEBI-

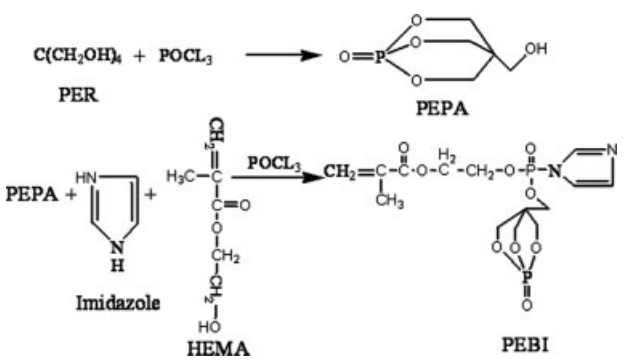

Scheme 1 Synthesis route of compound PEBI.

TABLE I
Sample Code and Compositions of the Composites

Sample code	PP (wt %)	OMT (wt %)	PB-OMT (wt %)	PP-*g*-MA (wt %)
PP0	100	0	0	0
PP1	97	3	0	0
PP2	97	0	3	0
PP3	82	0	3	15

OMT, and PP-*g*-MA, respectively, at 180°C in ThermoHaake Rheomix with a screw speed of 60 rpm, and the mixing time for each sample was 15 min. The mixed samples were transferred to a mold and preheated at 180°C for 5 min and then pressed at 15 MPa followed by cooling them to room temperature while maintaining the pressure for 5 min. The obtained sample sheets were used for further measurements. The sample code and the compositions are listed in Table I.

Characterization

Fourier transform infrared (FTIR) spectra of the samples were obtained on a VECTOR 22 FTIR Spectrometer (Bruker, Leipzig, Germany) in KBr pellets with a resolution of 4 cm^{-1}. X-ray diffraction (XRD) was carried out using a Rigaku X-ray generator (Cu Kα radiation with $\lambda = 1.54E$) at room temperature. The diffraction patterns were recorded at the scattering angles from 0.5° to 10° at a scanning rate of 2°/min.

To clarify the dispersion and nanostructure of clay in composites, a transmission electron microscope (TEM; JEM-1200EX) was used and operated at an accelerating voltage of 120 kV. The samples for TEM observation were ultrathin sectioned using a microtome equipped with a diamond knife. These sections (about 100 nm in thickness) were cut from a little piece of each sample and successively collected in a trough filled with water followed by placing them on 200-mesh copper grid.

Thermogravimetric analysis (TGA) was conducted by using a Pyris 6 TGA thermal analyzer (Perkin-Elmer, MA). Each specimen for testing with weight of about 10 mg was heated from 50 to 600°C at a linear heating rate of 10°C/min under N_2. Dynamic mechanical properties were performed using a dynamic mechanical analyzer (DMA242C). The tests were carried out in single-point bending mode at a vibration frequency of 2 Hz in a temperature range from −50 to 150°C at a heating rate of 5°C/min under nitrogen.

Cone calorimeter tests were performed using FTT, UK device according to ISO 5660 at an incident flux of 35 kW/m^2 using a cone-shaped heater. All samples for cone calorimeter measurements with the dimensions of 10 × 10 × 1.6 mm^3 were run in triplicate, and the average values were reported.

RESULTS AND DISCUSSION

FTIR analysis

The FTIR analysis was used to study whether PEBI could be grafted onto the PP backbones. PP/PEBI-OMT composite was first dissolved in the refluxing xylene, and the solution was filtered to remove the clay. Then, the filtrate was precipitated with acetone (poor solvent for PP). The precipitation was washed with acetone and water thrice, respectively, to remove the residual PEBI and dried at 80°C under vacuum for 12 h. The obtained product was designated as OMT-PEBI-*g*-PP.

The FTIR spectra for pure PP, PEBI, and PEBI-*g*-PP are presented in Figure 2. Numerous vibrations appeared in the spectrum of pure PP, the majority of which belonged to the —CH_2— and —CH_3 groups of the aliphatic chains. Compared with the spectrum of PP, except for the above characteristic peaks, a new absorbance peak at about 1725 cm^{-1}, which was assigned to C=O stretching vibration in compound PEBI, appeared in the spectrum for PEBI-*g*-PP, indicating that PEBI was successfully grafted onto the PP backbone chains. In addition, a weak new absorbance peak at about 670 cm^{-1} belonged to PEBI also appeared, which further confirmed the conclusion. As for the absorption bands at about 1550 cm^{-1}, 1300 cm^{-1}, and 1050 cm^{-1} attributed to PEBI did not appear in PP-*g*-PEBI, because the content of PEBI in PP-*g*-PEBI was so low that those bands could not be seen. The most important was that PEBI-grafted PP (PEBI-*g*-PP) could serve as a

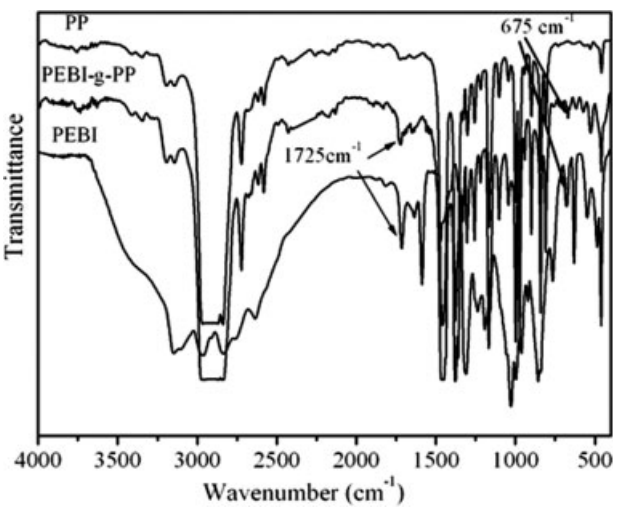

Figure 2 FTIR spectra for pure PP, PEBI-*g*-PP, and PEBI.

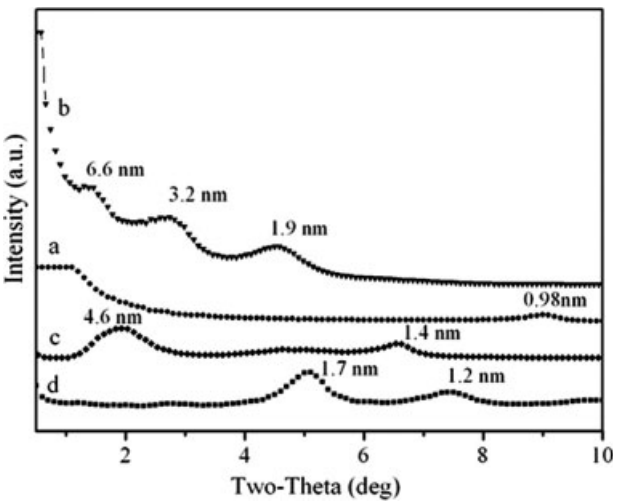

Figure 3 XRD patterns for (a) MMT, (b) OMT, (c) PB-OMT, and (d) HM-OMT.

compatibilizer between the PP and OMT, which would facilitate the dispersion of clay.

Intercalation effect of PB-OMT

XRD analysis is usually used to investigate the intercalated or exfoliated structure of clay. Figure 3 presents the XRD patterns for MMT, OMT, PB-OMT, and HM-OMT, respectively. MMT had a characteristic diffraction peak at 9.0° belonging to the (001) plane with a *d*-spacing of 0.98 nm, the intensity of diffraction peak is very small, because the intensities of diffraction peaks of other kinds of OMT were too strong. Compared with MMT, OMT showed three kinds of diffraction peaks corresponding to three intercalated structure with interlayer spacing of 1.9, 3.2, and 6.6 nm, respectively, which indicated that the clay existed in the form of different intercalated structure and the majority of clay existed in the form of former two kinds intercalated structure for the diffraction peak ($d = 6.6$ nm) was rather weak and blurry. Based on the organophilic environment of OMT, like epoxypropyl methacrylate,[18] PEBI could enter the clay galleries easily to increase the layer spacing further, thus relative to the former two clays, the basal spacing of PB-OMT (4.6 nm) was much larger, which clearly demonstrated the large steric volume effect of PEBI as cointercalation monomer. Moreover, the *d*-spacing value about 4.6 nm for PB-OMT was also far larger than that about 1.7 nm for HM-OMT, which might be explained by the following two reasons: one reason was that the polarity of HEMA molecule was so high that it could squeeze out an amount of organic parts in clay galleries and acted as an intercalating agent instead of bioctadecyl ammonium ions; the other reason was that its steric volume was far smaller than that of PEBI, so it could not increase the interlayer distance of clay like PEBI.

It was interesting that a small peak appeared at 6.5° ($d = 1.4$ nm), which indicated the collapse of partial OMT. As for the collapse of OMT, one possible reason was that the ammonium ions were extruded from the galleries by PEBI, because a very small peak at same location also appeared in XRD pattern for PB-OMT as shown in Figure 3.

Dispersion of PB-OMT in PP matrix

Figure 4 shows the XRD patterns for PP1, PP2, and PP3 nanocomposites. PP2 had a slightly larger basal spacing (about 4.0 nm) than that for PP1 (about 3.4 nm), which could be explained by the fact that PB-OMT had a larger interlayer distance than OMT and facilitated the dispersion of clay in the PP matrix. However, for PP2 that no PP chains entered the gallery of clay and partial PEBI molecules released, because the 001 reflection peak of clay is slightly shifted to a higher 2θ value with a *d*-spacing of 4.0 nm a little smaller than 4.6 nm of PB-OMT (Fig. 3). Taking into account that PP2 and PP3 had a strong diffraction peak at 6.5°, the position was the same as observed for PB-OMT (see Fig. 3). It was reasonable to believe that besides the reason mention earlier, another possible reason was that the thermal degradation of alkylammonium ions during the mixing process resulted in a slightly decrease in *d*-spacing of clay depressed.[18]

To further improve the dispersion of clay in PP matrix, PP-*g*-MA was introduced to serve as the primary compatibilizer. As expected, PP3 had a far larger interlayer distance (about 4.6 nm) than PP2 and PP1, indicating that the PP-*g*-MA molecular chains inserted the galleries of clay and the presence

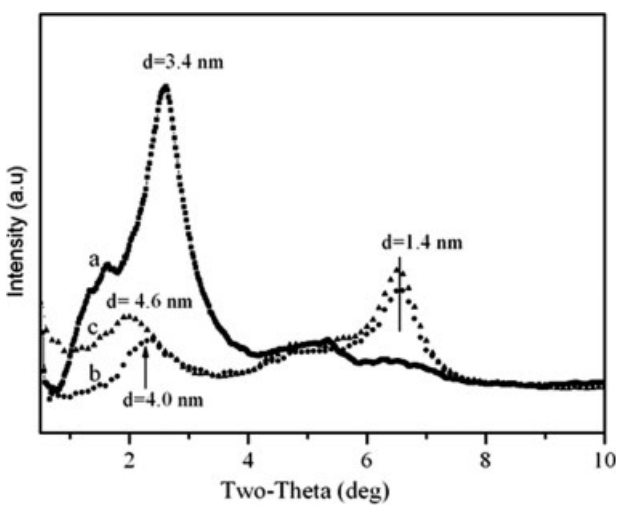

Figure 4 XRD patterns for (a) PP1, (b) PP2, and (c) PP3.

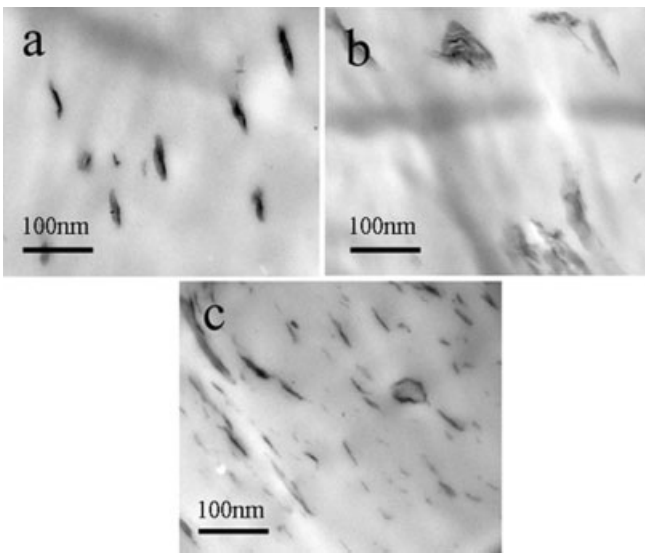

Figure 5 TEM images for three composites: (a) PP1, (b) PP2, and (c) PP3.

of PP-*g*-MA significantly improved the dispersion of clay in PP matrix.

To determine the dispersion of clay in polymer matrix, the utilization of XRDs alone is not enough. Because XRD is able to determine the basal interlayer spacing of clay, TEM allows for the direct imaging of the clay dispersion in polymer matrix. Figure 5 presents the TEM images of three samples. Compared with the TEM photo for PP1, PP2 had a better dispersion of clay in matrix because of less black tactoid in that for PP2. In contrast to both PP1 and PP2, the clay in PP3 dispersed more homogeneously and partial exfoliation could also be observed, all of which were in good agreement with the conclusion drawn from XRD analysis.

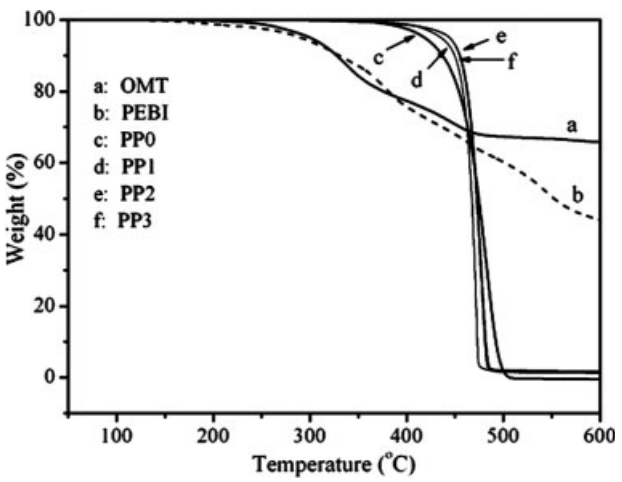

Figure 6 TGA curves for OMT, PEBI, pure PP, and three PP nanocomposites.

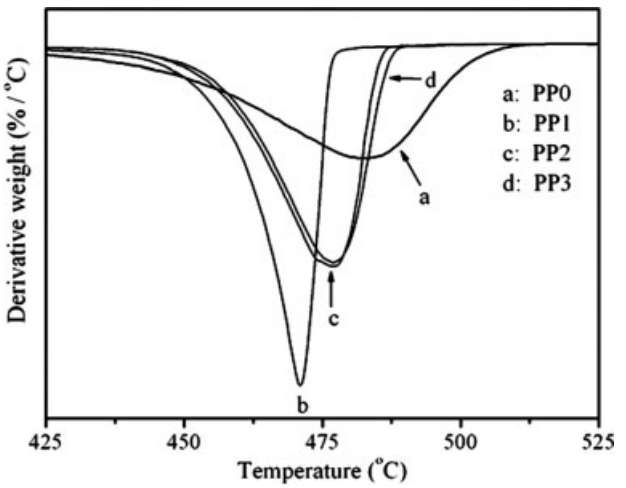

Figure 7 DTG curves for pure PP and three PP nanocomposites.

Thermal degradation

Thermal stability was an important property for which the nanocomposite morphology played an important role.[19] The thermal behaviors of PP nanocomposites were investigated with TGA and derivative TGA (DTG) at a heating rate of 10°C/min in N_2, and the results are shown in Figures 6 and 7, respectively. The detailed thermal degradation data are listed in Table II. The results revealed that although both the initial decomposition temperature (T_{onset}) and the temperature of maximum weight loss rate (T_{max}) for OMT and PEBI were about 100°C lower than those for pure PP, their char residues at 600°C were far more (65.6 wt % for OMT and 43.8 wt % for PEBI) than pure PP, because PP completely decomposed at 600°C without leaving any char. After incorporating 3 wt % clay into PP, initial decomposition temperature for PP1 was enhanced by about 17°C with a char yield of 1.3 wt %, which indicated that the thermal stability of PP hybrid was improved. When adding PB-OMT into pure PP at the same loading, the T_{onset} for PP composite was

TABLE II
Sample Code and Compositions of the Composites

Sample ID	T_{onset} (°C)	$T_{50\%}$ (°C)	T_{max} (°C)	Char residue at 600°C (wt %)
OMT	299	–	336	65.6
PEBI	290	552	379	43.8
PP0	418	474	483	
PP1	435	467	470	1.3
PP2	444	472	476	1.8
PP3	444	473	477	2.0

Notes: T_{onset}, initial decomposition temperature at which 5% weight loss occurred; $T_{50\%}$, the temperature at which 50% weight loss occurs; T_{max}, maximum weight loss temperature.

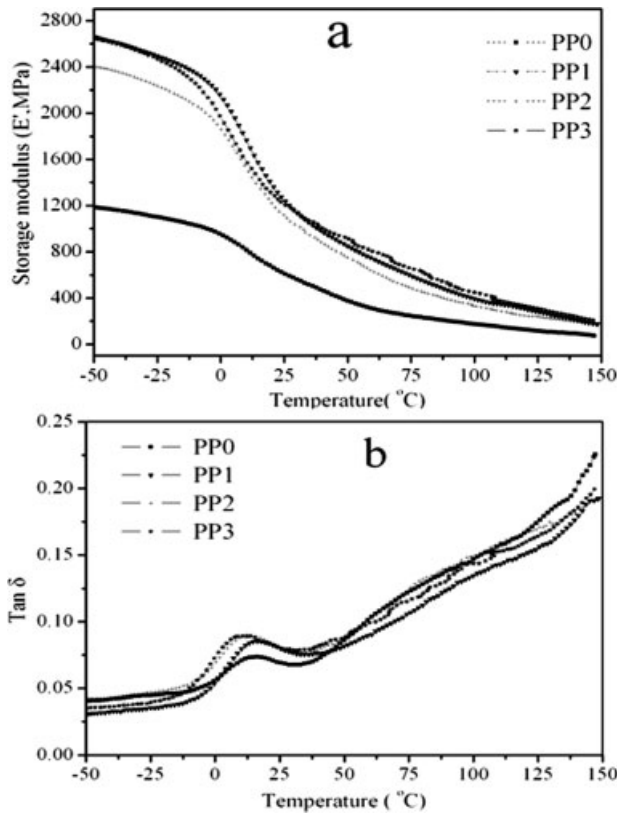

Figure 8 Dynamic mechanical spectra [(a) storage modulus E', (b) loss factor tan δ] as a function of temperature for PP and PP nanocomposites.

further elevated by about 26°C higher than that for pure PP, for which there were two kinds of possible interpretation, one was that the cointercalating effect of PEBI on clay led to the better dispersion of clay in PP matrix and a further increase in thermal stability for PP, the other was that only PEBI by itself improved the thermal stability. The introduction of the compatibilizer PP-*g*-MA did not further enhance the thermal stability of PP hybrid because of the same T_{onset} value as that for PP2 only having a slightly higher char residue about 2.0 wt %, which demonstrated the dispersion state of clay in matrix did not play an important role in the thermal properties for composites as we expected.

As for the temperature for half of sample decomposed ($T_{50\%}$) and the temperature for maximum weight loss (T_{max}), both temperatures for PP1, PP2, and PP3 were in some sort lower than those for pure PP, namely PP0, which could be explained by the fact that the lower T_{onset} for OMT and PEBI led to the lower $T_{50\%}$ and T_{max} for PP hybrids. As expected, both $T_{50\%}$ and T_{max} for PP2 and PP3 were about 5°C higher than those for PP1, one possible reason was that PEBI had higher T_{max} than OMT, which facilitated to improve the thermal stability of PP composites, and another cause was probably the cointercalating effect of PEBI and the good dispersion of clay in PP matrix, although it did not play a very important role.

Dynamic mechanical properties

Figure 8 presents the dynamic mechanical spectra (dynamic storage modulus E' and loss factor tan δ) as a function of temperature for PP and PP composites. McCrum et al. have demonstrated that the tan δ curve for pure PP exhibited three relaxations localized in the vicinity of −80°C (γ), 100°C (α), and 10°C (T_g), and the dominant relaxation appeared at about 10°C was the glass–rubber relaxation of the amorphous portion of PP.[20] Some values of E' and T_g at different temperatures for PP and PP hybrids are presented in Table III.

It was obviously observed from Table III that the incorporation of clay into PP matrix resulted in a considerable increase in stiffness for the storage modulus of PP hybrids about two times higher than that of PP0 in the testing temperature range indicating that the addition of clay resulting in a reinforcement effect. However, the E' curve for PP2 was slightly below that for PP1, which could be attributed to the plasticization effect of PP-*g*-PEBI. As for PP3, its storage modulus was higher than that for PP1, especially in higher temperature range, which was in good agreement with the results observed from TGA.

There was another interesting phenomenon that, except PP1, the values of T_g derived from the maximum values in tan δ curves for PP nanocomposites were lower than that for pure PP, which was in accordance with the results observed by Lin et al.,[17] but they did not give reasonable reasons. As shown in Table III, the better the dispersion extent of clay in matrix, the lower the T_g value. This phenomenon could be explained by the following facts.

Compared with pure PP, PP/OMT gave a higher T_g, which was consistent with the results reported.[6] By contraries, PP2 and PP3 gave a slightly lower T_g instead of a higher T_g. It is well known that the T_g of a polymer depends on the mobility of the chain

TABLE III
Dynamic Storage Modulus of Samples at Various Temperatures and the Values of T_g

	Storage modulus E' (MPa)				
Sample code	−45°C	25°C	85°C	145°C	T_g (°C)
PP0	1101.2	602.6	208.4	83.7	15.24
PP1	2492.1	1246.1	506.7	182.2	17.43
PP2	2229.2	1096.2	417.4	182.1	11.51
PP3	2472.3	1213.5	562.4	210.2	10.84

Notes: T_g was determined from the maximum in the tan δ versus temperature.

TABLE IV
Cone Calorimetric Analysis Data for PP0, PP1, PP2, and PP3 at 35 KW/m^2

	PP0	PP1	PP2	PP3
t_{ign} (s)	30	30	32	32
PHRR (kW/m^2)	390	185	170	161
AHRR (kW/m^2)	205	104	92	85
t_{PHRR} (s)	85	90	94	96
ASEA (m^2/kg)	555	440	400	380
AMLR (g/s)	0.035	0.029	0.028	0.025

Notes: t_{ign}, time to ignition; PHRR, peak heat release rate; AHRR, average heat release rate; t_{PHRR}, time to PHRR; ASEA, average-specific extinction area; AMLR, average mass loss rate.

segment of macromolecules in polymer matrix. If the molecular chains are restricted, motion or relaxation of the chain segments will become difficult, and the polymer will give a higher T_g value. When the PP molecular chains were intercalated into the silicate galleries or the partial clay was exfoliated in PP matrix, the chains conformation of PP molecules was not easily changed because of the sterical hindrances and the strong interaction between the polymer and the surface of the clay,[16] thus the PP/clay composites gave a higher T_g.

Unlike PP1, both PP2 and PP3 contained PB-OMT instead of OMT; thus, there were two opposite actions in both systems. PEBI-*g*-PP had large steric volume side groups that prevented effective packing of the polymer molecules and acted as an internal plasticization agent. This could be seen as the increase in local free volume, which allowed a higher molecular mobility and resulted in a decrease in T_g value.[17,21] In terms of PP2 and PP3 systems, except for the sterical hindrances and strong interaction between the polymer and the surface of the clay in PP matrix, there was a stronger internal plasticization effect. Furthermore, the latter dominated, and thus PP2 and PP3 systems exhibited a lower T_g value. PP3 had a slightly lower T_g value than PP2 did, which could be also dedicated to the plasticization effect of PP-*g*-MA because of its lower molecular weight than PP.

Flame-retardant properties analysis

To measure the flame retardancy of a material, cone calorimeter measurement is the most powerful tool to evaluate the flame retardancy performance so far, because it measures the most important single factor of a fire, called peak of heat release rate (PHRR). In Dubnikova's system,[18] the PHRR of nanocomposites PP/21 wt % MAPP/7 wt % clay was reduced to 41% of pure PP. Table IV shows that the PHRR value of PP/OMT nanocomposite was around 53% lower than that of pure PP (about 390 kJ/m^2), indicating the addition of OMT considerably improved the fire retardancy. Relative to PP/OMT nanocomposite, PP/PB-OMT composite gave much lower PHRR value (about 170 kJ/m^2, around 44% of that of pure PP), demonstrating that the incorporation of PEBI further enhanced the flame-retardancy property of PP, the phosphorus element in PEBI may be responsible for the improved flame retardancy, because phosphorus compounds were found to be effective flame retardants for PP.[21,22] Compared with PP0, PP1, and PP2, PP3, namely PP/PP-*g*-MA/PB-OMT composite gave a PHRR of 161kJ/m^2, exhibited the best flame-retardancy property, which could be explained by the fact that PP-*g*-MA, the primary compatibilizer, facilitated the dispersion of PB-OMT in PP matrix and thus further raised the flame-retardant property of materials.

CONCLUSIONS

In this article, a series of PP nanocomposites were successfully prepared by *in situ* grafting intercalation of a novel cointercalating monomer using PP-*g*-MA as the primary compatibilizer via melt blending. The incorporation of cointercalation monomer PEBI into OMT composites significantly increased the basal interlayer spacing of clay and subsequently facilitated the dispersion of clay in PP matrix because of its great bulky character and improves the flame retardancy properties of PP on the basis of PP/OMT composites. The thermal stability of PP hybrids was considerably enhanced with the addition of PEBI. For PP/OMT hybrids, the storage modulus was significantly enhanced and the T_g shifted to a slightly lower temperature with the incorporation of clay for PP/OMT hybrids. PP/PB-OMT composites gave a lower T_g value because of its plasticization effect. PP/PB-OMT/PP-*g*-MA hybrid has a far lower T_g value than did PP2, because the PP-*g*-MA had a lower molecular weight than PP and also displayed internal plasticization effect. Cone calorimeter results show that the incorporation of PEBI could highly improve the flame-retardancy properties of PP, because the PHRR value of PP/PB-OMT/PP-*g*-MA hybrid was 58% lower than that of pure PP.

References

1. Alexandre, M.; Dubois, P. Mater Sci Eng 2000, 28, 1.
2. Messersmit, P.; Giannelis, E. J Polym Sci A 1995, 33, 1047.
3. Suprakas, S. R.; Okamoto, M. Prog Polym Sci 2003, 28, 1539.
4. Kashiwagi, T.; Harris, R. H.; Zhang, X.; Briber, R. M.; Cipriano, B. H. Polymer 2004, 45, 881.
5. Kim, J. H.; Koo, C. M.; Choi, Y. S.; Wang, K. H.; Chung, I. J Polym 2004, 45, 7719.
6. Tidjani, A.; Wald, O.; Martina, M. P.; Manfred, P. Polym Degrad Stab 2003, 82, 133.
7. Zanetti. M.; Bracco, P.; Costa, L. Polym Degrad Stab 2004, 85, 657.

8. Morlat, S.; Maihot, B.; Gonzalez, D.; Gardette, J. L. Chem Mater 2004, 16, 377.
9. Gopakumar, T. G.; Lee, J. A.; Kongtopoulou, M.; Parent, J. S. Polymer 2002, 43, 5438.
10. Lu, H. D.; Hu, Y.; Kong, Q. H.; Cai, Y. B.; Chen, Z. Y.; Fan, W. C. Polym Adv Technol 2004, 15, 601.
11. Carrado, K. A.; Xu, L. Chem Mater 1998, 10, 1440.
12. Tao, S.; Juan, M. G. Adv Mater 2002, 14, 128.
13. Giannelis, E. P. Adv Mater 1996, 8, 29.
14. Weimer, M. W.; Chen, H.; Giannelis, E. P.; Sogah, D. Y. J Am Chem Soc 1999, 121, 1615.
15. Masaya, K.; Naoki, H.; Makoto, K.; Arimitsu, U.; Akane, O. Macromolecules 1997, 30, 6333.
16. Zhang, Y. Q.; Lee, J. H.; Jang, H. J.; Nah, C. W. Compos B 2004, 35, 133.
17. Lin, X. H.; Wu, Q. J Polym 2001, 42, 10013.
18. Dubnikova, I. L.; Berezina, S. M.; Yu, M. K.; Kim, G. M.; Lomakin, S. M. J Appl Polym Sci 2007, 105, 3834.
19. Kilburn, D.; Dlubek, G.; Pionteck, J.; Alam, M. A. Polymer 2006, 47, 7774.
20. McCrum, N. G.; Read, B. E.; Williams, G. Anelastic and Dielectric Effects in Polymeric Solids; Wiley: London, 1967.
21. Mikroyannidis, J. A.; Kourtides, D. A. J Appl Polym Sci 1984, 29, 941.
22. Liu, W. C.; Varley, R. J.; Simon, G. P. J Appl Polym Sci 2004, 92, 2093.